J Solid State Electrochem (2011) 15:2645–2652
DOI 10.1007/s10008-010-1256-9

ORIGINAL PAPER

Three-dimensional nanocarbon and the electrochemistry of nanocarbon/tin oxide for lithium ion batteries

Chaofeng Zhang · Matt Quince · Zhixin Chen · Zaiping Guo · Huakun Liu

Received: 27 September 2010 / Revised: 14 November 2010 / Accepted: 15 November 2010 / Published online: 1 December 2010

Abstract In this work, the potential of using coconut shell, which is very cheap and readily available, for the production of graphitic nanocarbon three-dimensional networks is investigated. The three-dimensional carbon has been produced via the wet-impregnation of coconut shell powder with a transition metal catalyst. The novel process employed offers low costs and environmental advantages, with biological waste used in place of carbonaceous precursor as the feedstock. Nanocarbon/tin oxide composites were prepared via wet-impregnation and the solvothermal method, using tin chloride solution with the activated nanocarbon. The electrochemical performances of the three-dimensional nanocarbon doped with tin oxide and of activated nanocarbon alone as anode materials were investigated in rechargeable lithium ion batteries. One composite made by using the solvothermal method shows stable cyclic retention up to 100 cycles and delivers a high reversible capacity of about 405 mAh g^{-1}.

Keywords Coconut shell · 3-D nanocarbon · Lithium ion batteries · Tin oxide

C. Zhang · M. Quince · Z. Chen · Z. Guo (✉)
School of Mechanical, Materials & Mechatronics Engineering,
University of Wollongong,
Wollongong, NSW 2522, Australia
e-mail: zguo@uow.edu.au

C. Zhang
e-mail: cfezhang@foxmail.com

C. Zhang · Z. Guo · H. Liu
Institute for Superconducting & Electronic Materials,
University of Wollongong,
Wollongong, NSW 2522, Australia

Introduction

Rechargeable lithium ion batteries are currently regarded as the power source of choice for portable electric devices and hybrid electric vehicles [1, 2]. Tin-based oxides have been proposed as potential substitutes for the graphite anode material currently used in rechargeable lithium batteries, due to their higher theoretical reversible specific capacity (782 mAh g^{-1} for SnO_2), which is more than twice that of graphite (372 mAh g^{-1}) [3]. To date, the main challenge for the commercial use of tin oxide is its poor cycling performance, which is caused by the huge volume variation during the Li^+ insertion/extraction cycle, which results in pulverization of the electrode and rapid capacity decay. Many methods have been investigated to resolve the above so-called "volume change" problem [4–6]. Tin oxide materials fabricated into special nanostructures, such as nanorods [7, 8], nanowires [9, 10], and hollow spheres [11–13], can effectively enhance the electrochemical performance. However, the high cost of preparing such nanostructured materials restricts their wide commercial application. Other strategies for coating/adding active/inactive materials (such as carbon) inside or outside the particles have been investigated and have been found to give better electrochemical performance than the bare materials [14, 15]. Carbon has been considered as the best choice for the coating/additive material, not only because it is light, but also because it can increase the electronic conductivity of the nanocomposite electrode and buffer the stress induced by volume expansion/contraction [16–21]. It is highly important to find economical methods for synthesizing SnO_2/C composite.

Current methods adopted for the preparation of nanocarbon materials are commonly characterized by high cost and the need for high quality carbonaceous precursor gases [22]. There is a high demand to seek renewable and cheap sources, which would be helpful for enabling the sustainable development of our society. In general, plants have their natural hierarchal structure. Mesoporous materials made from hierarchical biological structures as templates have attracted considerable interest. Coconut shell is a common lignocellulosic carbonaceous material consisting mainly of hemicellulose, cellulose, and lignin, with traces of other elemental species, usually present as oxides. Structurally, coconut shell is composed of numerous interconnected cells, which link together to form cylindrical tubes approximately 10 μm in diameter. After carbonization, the hierarchal pore structure is retained, which can provide an ideal hierarchal porous carbon framework supporting various functional nanoparticles for many different applications. For example, high-surface-area activated carbon was prepared from coconut shell fibers [23, 24]. The carbon made from coconut shell has been investigated as an adsorbent, catalyst (iron-embedded activated carbon), additive material in lithium ion batteries, etc. [24–30]. As an additive material, the electrical conductivity of carbon is very important to the electrochemical performance of anode materials. The electrical conductivity of the hierarchal carbon could be improved by introducing a graphite network on the carbon surface.

In the present work, hierarchal carbon networks were synthesized from coconut shell and then decorated with nano-SnO_2 particles. The three-dimensional (3-D) nanocarbon can be prepared on a large scale and at a low price compared to carbon nanotubes (CNTs), and can replace CNTs as the conducting matrix and volume buffering agent in the C/SnO_2 composites, which are promising anode materials for lithium ion batteries. The electrochemical performances of the as-prepared C/SnO_2 composites for lithium ion batteries were investigated and compared with that of bare SnO_2.

Experimental

Preparation of samples

All chemicals were purchased from Sigma-Aldrich Co. Ltd. Coconut shells purchased from the supermarket were broken into pieces of less than 2 cm along their largest dimension and then dried in an oven in air at 105 °C for 24 h, which was followed by grinding for 30 s. The powder was sized using a sieve with a mesh size of <106 μm. One gram of ground coconut shell powder was impregnated with ferric nitrate solution, which was prepared by combining 2.2 ml of distilled water and 0.55 g of Fe $(NO_3)_3 \cdot 9H_2O$ under vacuum. The resultant samples were heated from ambient temperature to 800 °C at a heating rate of 10 °C/min while maintaining the vacuum. The samples were held at this temperature for 90 min and then furnace cooled. The samples were activated by impregnation of potassium hydroxide prior to the heat treatment process. Activated samples were washed to remove the iron using 16% hydrochloric acid, and then filtered and washed numerous times with distilled water to remove any residual HCl solution, followed by drying in air at 80 °C for 24 h.

The activated samples were decorated with tin oxide using the two following processes. In the impregnation process, 0.27 g of the prepared nanocarbon was dispersed in distilled water, and 1.0 g $SnCl_2 \cdot 2H_2O$ was dissolved in ethanol and then mixed with the carbon dispersion. The mixture was further dispersed by ultrasonication for 5 h and then was dried in an oven in air at 80 °C for 2 days. The obtained sample was heat-treated for 6 h at 500 °C in vacuum in a tube furnace, with a heating rate of 10 °C/min, and then furnace cooled to room temperature. The sample thus obtained was designated as Imp-SnO_2/C. A bare SnO_2 sample was prepared in the same way, but in the absence of any nanocarbon.

The solvothermal samples designated Sl-SnO_2/C and Sh-SnO_2/C were prepared by the following method [31]. The nanocarbon was added into a solution of $SnCl_2 \cdot 2H_2O$ dissolved in ethanol with molar ratios of C:Sn of 1:0.1 (Sl-SnO_2/C) and 1:0.3 (Sh-SnO_2/C), respectively. The suspensions were further dispersed by ultrasonication for 90 min, and then were transferred into autoclaves and kept at 150 °C for 10 h. The products were washed with distilled water, dried, and heat-treated in a tube furnace at 350 °C for 10 min with natural cooling.

Sample characterization

The microstructure and morphology of the as-prepared nanocarbon and SnO_2/C composites were characterized by X-ray diffraction (XRD; GBC MMA 017), the Brunauer–Emmett–Teller technique (BET; Quanta Chrome Nova 1,000), scanning electron microscopy (SEM; JEOL JSM 6460A, with JEOL energy-dispersive X-ray (EDX) spectroscopy and an EDX mapping system), and transmission electron microscopy (TEM; JEOL 2011, 200 KV). The thermal properties of the as-prepared SnO_2/C composites were characterized by thermogravimetric analysis (TGA; TA Instruments 2,000).

Electrochemical measurements

The working electrodes were prepared by mixing 70 wt.% as-prepared SnO_2/C active material with 15 wt.% carbon

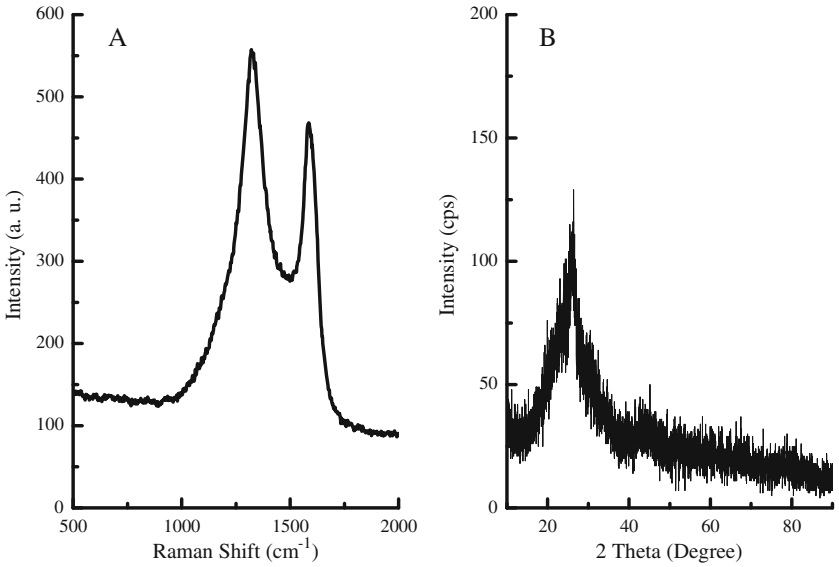

Fig. 1 **a** Raman spectrum and **b** XRD pattern of nanocarbon

black and 15 wt.% polyvinylidene difluoride binder in *N*-methyl-2-pyrrolidinone to form a homogeneous slurry, which was uniformly pasted onto nickel foam. The prepared working electrodes were dried in a vacuum oven at 100 °C for over 12 h and were pressed; they then were ready to be assembled into a testing cell. Electrochemical cells (CR2032 coin type) using the C/SnO_2 composite as working electrode, Li foil as the counter electrode and reference electrode, a microporous polypropylene film as the separator, and 1 M $LiPF_6$ in a 1:1 (*v*/*v*) mixture of ethylene carbonate and diethyl carbonate as the electrolyte were assembled in an Ar-filled glove box (H_2O, O_2< 0.1 ppm, Mbraun, Unilab, USA). The cells were galvanostatically charged and discharged over a voltage range of 0.01–3 V versus Li/Li^+ at a constant current density of 156 mA g^{-1}, based on the weight of the composite on a Land CT2001A cycler.

Results and discussions

The nanocarbon was characterized by Raman spectroscopy and XRD (Fig. 1). Peaks appear in the XRD pattern of the nanocarbon at about 26° and 43°, which correspond to the (002) and (101) reflections of carbon, respectively. From the Raman spectrum, it can be seen that the main broad bands appear at about 1,335 cm^{-1} (*D* band) and 1,587 cm^{-1} (*G* band), which are ascribed to the carbon inactive A_{1g} and active E_{2g} modes, respectively. The *D*/*G* intensity ratio is ~2.5, which indicates that the majority of the nanocarbon is amorphous [32–34]. 121.8 m^2/g of measured BET surface area and 0.9995 for the BET function coefficient were obtained when the material was carbonized at 800 °C for 90 min.

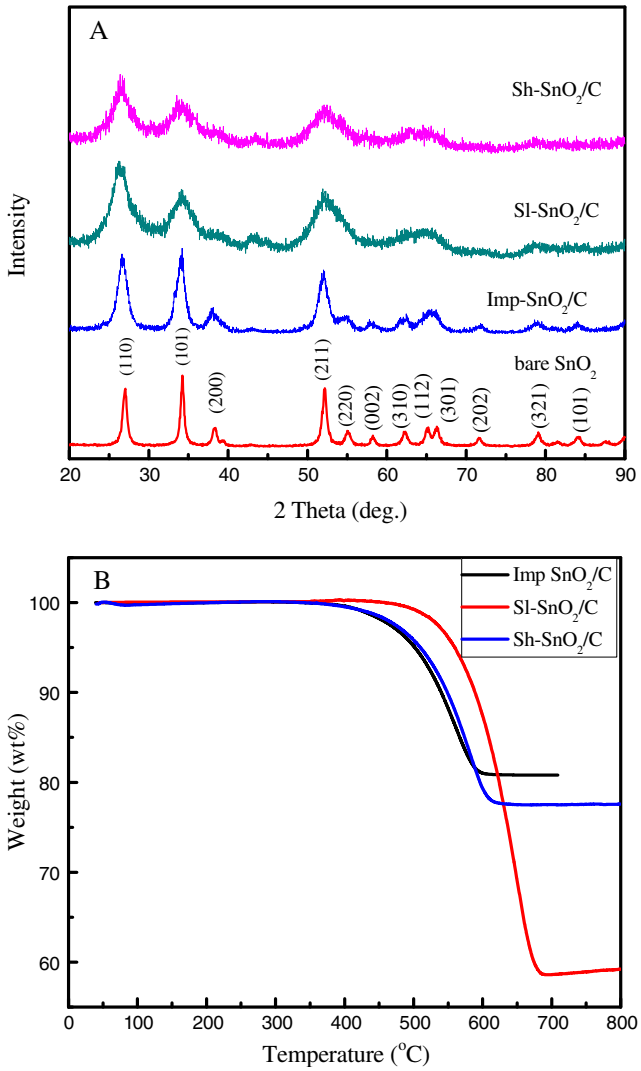

Fig. 2 **a** XRD patterns of SnO_2/C composites, and **b** TGA curves showing the weight losses of the three SnO_2/C samples

The structural features of the nanocarbon/tin oxide composites were also characterized by XRD and are shown in Fig. 2a, which demonstrates that the tin oxide in the bare SnO_2, Imp-SnO_2/C, Sl-SnO_2/C, and Sh-SnO_2/C samples has the same crystal structure as tetragonal rutile SnO_2 (JCPDS card No. 41–1,445, space group: $P4_2/mnm$, $a=b=$ 4.738 Å, $c=3.187$ Å). For the Imp-SnO_2/C, Sl-SnO_2/C, and Sh-SnO_2/C samples, peaks at 26.5°, 34.0°, and 52.0° correspond to the (110), (101), and (211) reflections of SnO_2, respectively. As can be seen, no carbon peaks can be found in the XRD patterns of the SnO_2/C composites, indicating the amorphous nature of the carbon in these samples and the highly crystalline structure of the SnO_2.

TGA was used to quantitatively evaluate the amount of carbon present in the as-prepared SnO_2/C products. Figure 2 (b) shows that the weight loss mainly occurred between 300 and 700 °C. The ratio of carbon to tin oxide can be determined to be about 20:80, 42:58, and 22:78 by weight for Imp-SnO_2/C, Sl-SnO_2/C and Sh-SnO_2/C, respectively. The results basically agree with the nominal ratios of precursors, nanocarbon, and $SnCl_2$.

SEM and TEM images of the nanocarbon are shown in Fig. 3. A hierarchical pore structure with a network of continually interconnected pores of progressively smaller volume was observed. Detection of the catalyst was in trace amounts only, and is not discernible in the EDX spectra (not displayed here). From Fig. 3b, it can be seen that there are numerous carbon sheet structures around the nanocarbon. Figure 3c shows a high magnification image of the nanocarbon, which gives the typical lattice fringes of carbon.

After the tin oxide decoration using the impregnation method, the morphology is not same as that of the initial sample. Figure 4a and b present TEM images of Imp-SnO_2/

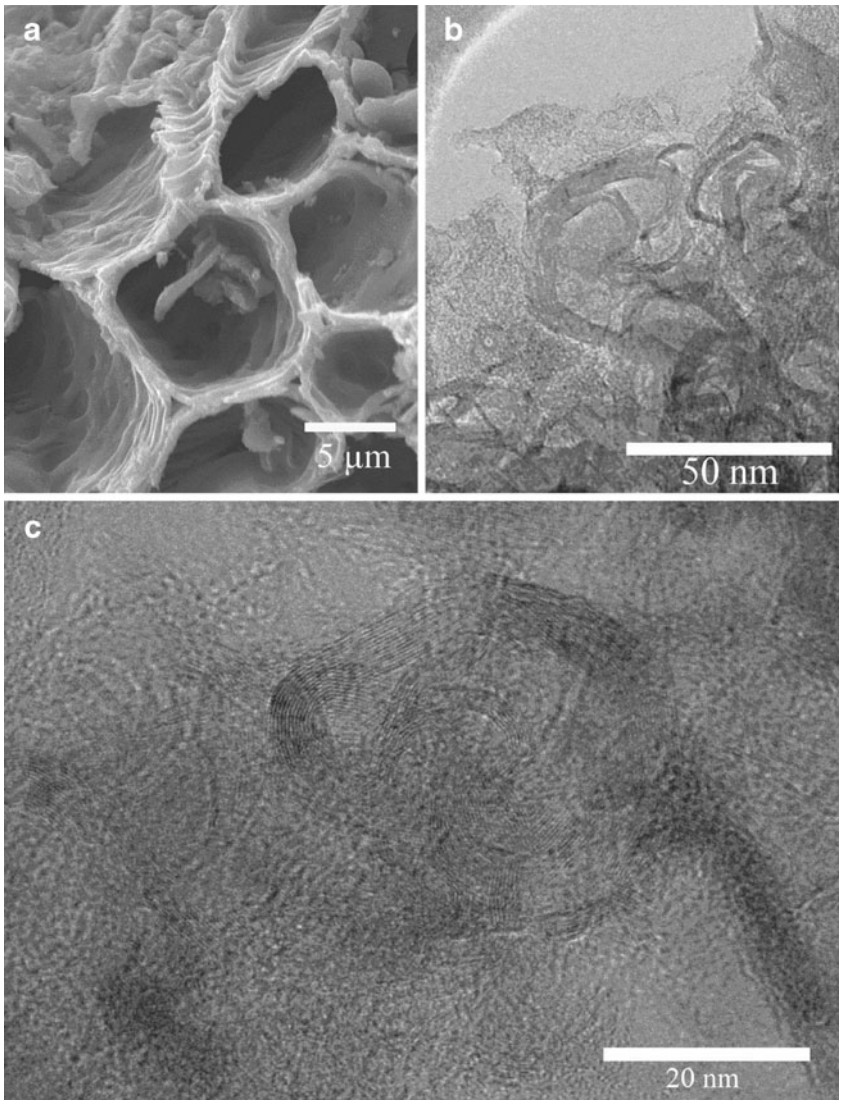

Fig. 3 SEM (**a**, **b**) and TEM (**c**) images of nanocarbon networks

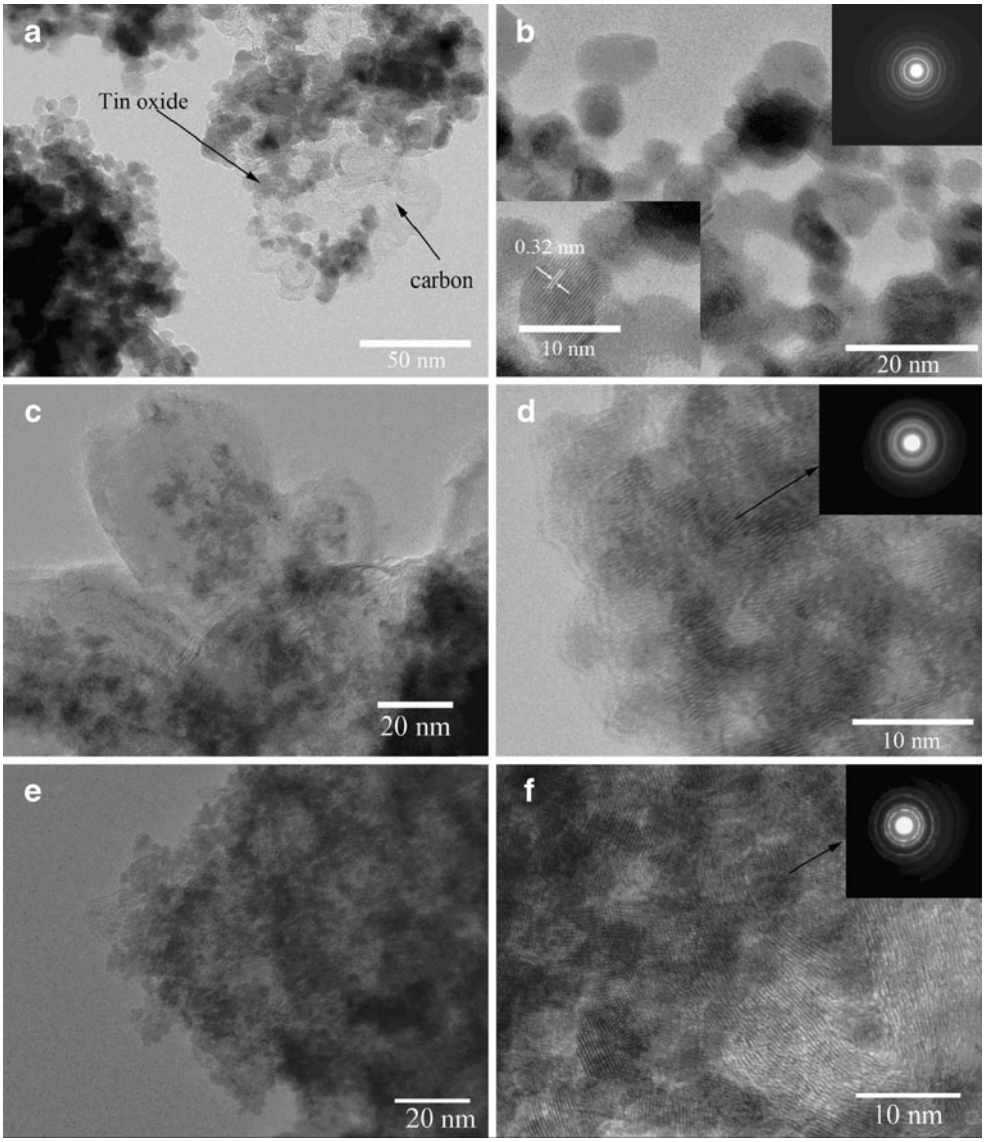

Fig. 4 **a** and **b** TEM and HRTEM (*lower left inset* of (**b**)) images of Imp-SnO_2/C nanocomposite, with the *upper right inset* in (**b**) showing the corresponding SAED pattern of the tin oxide; **c** and **d** TEM and HRTEM images of Sl-SnO_2/C; with the *inset* (**d**) showing the corresponding SAED pattern of the tin oxide; **e** and **f** TEM and HRTEM images of Sh-SnO_2/C, with the *inset* (**f**) showing the corresponding SAED pattern of the tin oxide

C. A dispersion of tin-rich particles, typically 5–10 nm in diameter, throughout a nanocarbon matrix constituted the majority of the Imp-SnO_2/C sample from TEM observations and analysis. Figure 4a shows the typical fine dispersion of particles, as well as a region of larger tin-rich particles. Figure 4b shows a high-resolution TEM (HRTEM) image of the lattice fringes of crystalline SnO_2 particles. The selected area electron diffraction (SAED) patterns of large numbers of tin oxide particles can be indexed as SnO_2, which is consistent with the results of the XRD analysis. The corresponding SAED pattern in the inset of Fig. 4b verifies the crystalline nature of the tin-rich particles. The plane spacing is 0.32 nm, which is the *d*-spacing of (110) planes of SnO_2.

Figure 4c and e show images of Sl-SnO_2/C, and Sh-SnO_2/C composites synthesized by using the solvothermal method. The composites consist of large lumps of amorphous carbon with SnO_2 particles on their surface. Since the SnO_2 particles are poor electrical conductors, they appear bright in secondary electron images due to charging effects. It can be seen that the surface of the amorphous carbon is decorated with nanocarbon and a large number of tin oxide particles a few nanometers in diameter. Numerous such particles were observed with diameters of less than 10 nm. As expected, the tin oxide coated composites have the morphology where the tin oxide covers the nanocarbon. The distribution and morphology of the two samples were further analyzed by HRTEM. Both samples show that the crystal size of SnO_2 is around 5 nm. With an increasing ratio of $SnCl_2$ in the precursors, the content of tin oxide in the final composite also increases, as seen from Fig. 4c and e, and the crystallinity of the tin oxide is higher, as can be inferred from the insets of Fig. 4d and f.

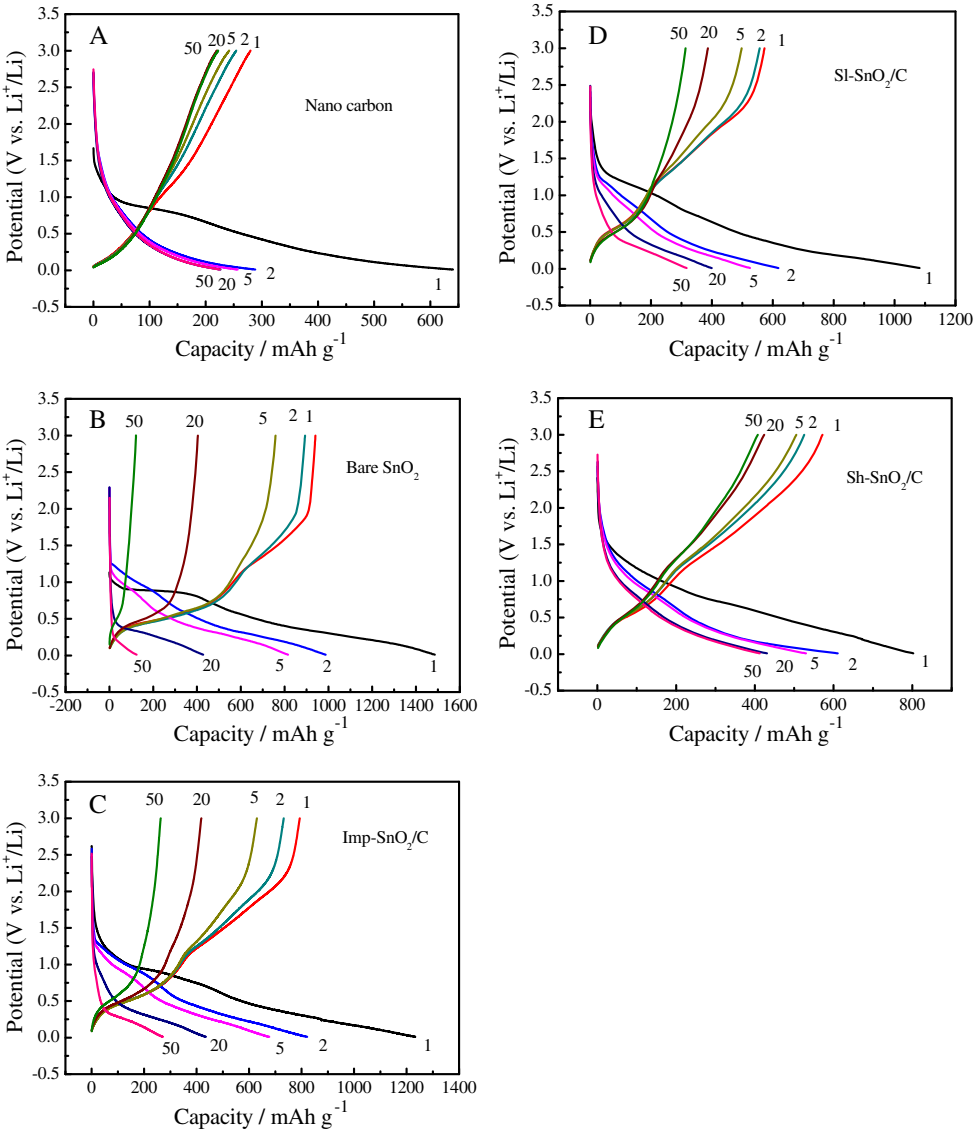

Fig. 5 Discharge–charge curves of **a** nanocarbon, **b** bare SnO_2, **c** Imp-SnO_2/C, **d** Sl-SnO_2/C, and **e** Sh-SnO_2/C for selected cycles

Figure 5 shows the discharge–charge curves of nanocarbon, bare tin oxide, Imp-SnO_2/C, Sl-SnO_2/C, and Sh-SnO_2/C electrodes cycled between 0.01 and 3.0 V vs. Li/Li^+ at 0.2 C (156 mA g^{-1}). The first discharge delivered specific capacities of 640, 1,485, 1,299, 1,170, and 893 mAh g^{-1}, respectively. From Fig. 5a, it can be seen that the voltage profile is composed of two parts: one is the slope region at high voltage (V>0.5 V), which is ascribed to the formation of the solid electrolyte interphase (SEI) layer and the filling of the micropores with lithium [35], while the other is the lower potential (V<0.5 V) region, which is due to lithium in the carbon sheets and edges [3, 36].

After decorating with tin oxide, the curves are similar to what has been previously reported [14, 31]. The anode materials have irreversible capacities, as can be seen from Fig. 5c–e. The reasons for the phenomenon of initial irreversible capacity are the formation of the SEI layer at around 0.8 V (vs. Li^+/Li) and the irreversible reaction from SnO_2 to Sn in the first cycle (Eq. 1). SnO_2 reacts with lithium in a two-step process, given by Eqs. 1 and 2:

$$SnO_2 + 4Li^+ + 4e^- \rightarrow Sn + 2Li_2O\left(707\,mAhg^{-1}\right) \quad (1)$$

$$Sn + xLi^+ + xe^- \leftrightarrow LixSn\left(0 \le \times \le 4.4,\ 993\ mAhg^{-1}\right) \quad (2)$$

Figure 5b shows that the 100th discharge capacity of bare SnO_2 is about 23 mAh g^{-1}. However, the 100th cycle discharge capacity of Sh-SnO_2/C is around 405 mAh g^{-1}, which is can be seen from Fig. 5e. Comparing Fig. 5e with Fig. 5b, it can be inferred that the 100th discharge capacity

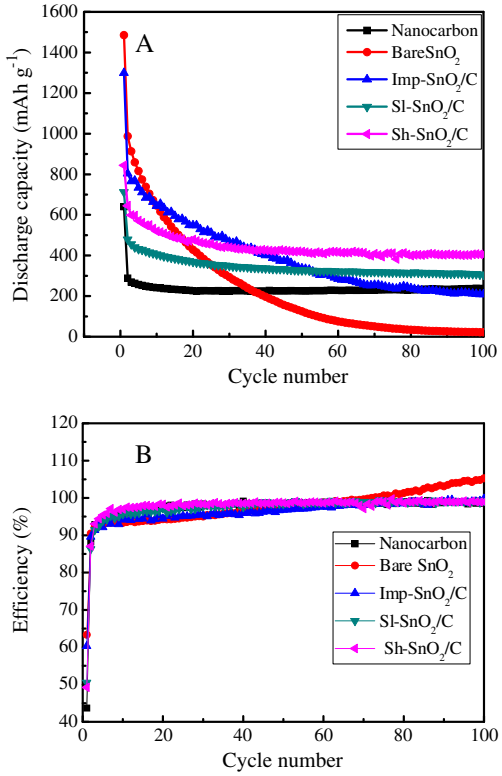

Fig. 6 Electrochemical performance **a** and coulombic efficiency **b** of nanocarbon, bare SnO_2, Imp-SnO_2/C, Sl-SnO_2/C, and Sh-SnO_2/C

of bare SnO_2 is about 6% of that of Sh-SnO_2/C. The initial coulombic efficiencies of nanocarbon, bare SnO_2, Imp-SnO_2/C, Sl-SnO_2/C, and Sh-SnO_2/C are 43%, 63%, 58%, 53%, and 70%, respectively (Fig. 6a). For the as-prepared three-dimensional nanocarbon, the discharge capacity drops in the first 10 cycles and then remains at around 237 mAh g^{-1} until the 100th cycle. The discharge capacity of bare SnO_2 powder decreases gradually to 23 mAh g^{-1} in the 100th cycle. The capacities of Imp-SnO_2/C, Sl-SnO_2/C, and Sh-SnO_2/C remain at 208, 306, and 405 mAh g^{-1}, respectively, even up to 100 cycles (Fig. 6 (a)). The sheet-like structure of three-dimensional nanocarbon not only can improve the electrical conductivity, but also can buffer the volume change. With decreasing particle size of SnO_2, the absolute volume change drops. The decrease in the absolute volume change is beneficial to the retention of discharge capacity. From the TEM and XRD results, it can be inferred that the particle size decreases in the order from Imp-SnO_2 to Sl-SnO_2 to Sh-SnO_2 [31, 37, 38]. Both of these characteristics enhance the electrochemical performance during lithium insertion and extraction. Both Sl-SnO_2/C and Sh-SnO_2/C anode materials show stable capacity retention, with Sh-SnO_2 giving higher capacity. Figure 6a shows that the samples made by the solvothermal method have better capacity retention than the sample produced by using the impregnation method. The main reason is that the higher pressure created in the solvothermal process can pin SnO_2 to the nanocarbon, which could efficiently prevent the agglomeration of SnO_2. However, the SnO_2 is only loaded on the nanocarbon in the impregnation process. Compared with other SnO_2/C composites used for lithium ion batteries [31, 39–41], the 3-D nanocarbon/SnO_2 composites have some advantages, such as that the 3-D nanocarbon can be easily fabricated on a large scale via the wet-impregnation of coconut shell powder with a transition metal catalyst, followed by sintering. Therefore, the 3-D nanocarbon we used here is much cheaper than CNTs, which have been widely used in SnO_2/C composites as anode materials for lithium ion batteries. The SnO_2/C is able to deliver a capacity of 405 mAh g^{-1}, even after 100 charge–discharge cycles, which is comparable to or even better than the performance of the SnO_2/CNTs reported so far [31, 39–41].

Conclusions

In this study, a wet-impregnation method for producing three-dimensional nanocarbon materials from coconut shell is reported. The composites contain both 3-D nanocarbon as a carrier and tin oxide incorporated by two different methods, wet-impregnation and the solvothermal method. Their electrochemical performances were investigated for lithium ion batteries. The composite with the higher tin oxide content that was made by using the solvothermal method shows stable cyclic retention up to 100 cycles and delivers a high reversible capacity of about 405 mAh g^{-1}. The three-dimensional nanocarbon material made from cheap coconut can be suggested as a promising material to replace the nanocarbon materials prepared by using chemical vapor deposition and other high cost methods.

Acknowledgments Financial support provided by the Australian Research Council (ARC) through an ARC Discovery project (DP0878611) is gratefully acknowledged. The authors would like to thank Dr. Jun Liu, Dr. Shulei Chou, and Mr. Peng Zhang and Mr. Chung-Kiak Poh at the University of Wollongong for their assistance in using laboratory equipment and valuable remarks. We would also like to thank Dr. Tania Silver for editing the manuscript.

References

1. Tarascon JM, Armand M (2001) Nature 414:359
2. Winter M, Brodd RJ (2004) Chem Rev 104:4245
3. Dahn JR, Zheng T, Liu YH, Xue JS (1995) Science 270:590
4. Beaulieu LY, Eberman KW, Turner RL, Krause LJ, Dahn JR (2001) Electrochem Solid State Lett 4:A137

5. Fransson L, Nordstrom E, Edstrom K, Haggstrom L, Vaughey JT, Thackeray MM (2002) J Electrochem Soc 149:A736
6. Veeraraghavan B, Durairajan A, Haran B, Popov B, Guidotti R (2002) J Electrochem Soc 149:A675
7. Wang Y, Lee JY (2004) J Phys Chem B 108:17832
8. Zhang YL, Liu Y, Liu ML (2006) Chem Mater 18:4643
9. Kim H, Cho J (2008) J Mater Chem 18:771
10. Ying Z, Wan Q, Cao H, Song ZT, Feng SL (2005) Appl Phys Lett 87:113108
11. Lou XW, Wang Y, Yuan CL, Lee JY, Archer LA (2006) Adv Mater 18:2325
12. Yang HX, Qian JF, Chen ZX, Ai XP, Cao YL (2007) J Phys Chem C 111:14067
13. Liu HM, Wang YG, Wang KX, Hosono E, Zhou HS (2009) J Mater Chem 19:2835
14. Chou SL, Wang JZ, Zhong C, Rahman MM, Liu HK, Dou SX (2009) Electrochim Acta 54:7519
15. Kaskhedikar NA, Maier J (2009) Adv Mater 21:2664
16. Chen JS, Cheah YL, Chen YT, Jayaprakash N, Madhavi S, Yang YH, Lou XW (2009) J Phys Chem C 113:20504
17. Courtel FM, Baranova EA, Abu-Lebdeh Y, Davidson IJ (2010) J Power Sources 195:2355
18. Park MS, Kang YM, Kim JH, Wang GX (2008) Adv Funct Mater 18:455
19. Wang Y, Su FB, Lee JY, Zhao XS (2006) Chem Mater 18:1347
20. Zhang WM, Hu JS, Guo YG, Zheng SF, Zhong LS, Song WG, Wan LJ (2008) Adv Mater 20:1160
21. Cui GL, Hu YS, Zhi LJ, Wu DQ, Lieberwirth I, Maier J, Mullen K (2007) Small 3:2066
22. O'Connell MJ (2006) Carbon nanotubes: properties and applications. CRC, Boca Raton
23. Chen Y, Zhou LJ, Hong YZ, Cao F, Li L, Li JB (2010) New Carbon Mater 25:151
24. Jurewicz K, Babel K (2010) Energ Fuel 24:3429
25. Gottipati R, Mishra S (2010) Chem Eng J 160:99
26. Ochiai R, Uddin MA, Sasaoka E, Wu SJ (2010) Energ Fuel 23:4734
27. Guo MX, Qiu GN, Song WP (2010) Waste Manage 30:308
28. Liou RM, Chen SH, Huang CH, Hung MY, Chang JS, Lai CL (2010) Water Sci Technol 61:1489
29. Fang ZQ, Huang HJ (2010) Adsorpt Sci Technol 27:685
30. Hwang YJ, Jeong SK, Shin JS, Nahm KS, Stephan AM (2008) J Alloy Compd 448:141
31. Du GD, Zhong C, Zhang P, Guo Z, Chen ZX, Liu HK (2010) Electrochim Acta 55:2582
32. Wang H, Dai Q, Li Q, Yang J, Zhong X, Huang Y, Zhang A, Yan Z (2009) Solid State Ionics 180:1429
33. Doi T, Miyatake K, Iriyama Y, Abe T, Ogumi Z, Nishizawa T (2004) Carbon 42:3183
34. Lee KT, Lytle JC, Ergang NS, Oh SM, Stein A (2005) Adv Funct Mater 15:547
35. Stevens DA, Dahn JR (2000) J Electrochem Soc 147:4428
36. Nishi Y (2001) Chem Rec 1:406
37. Wu SY, Chen XM, Chen LM (2008) J Electroceram 21:810
38. Byrappa K, Ohachi T (2003) Crystal growth technology. William Andrew, New York
39. Zhao NH, Yang LC, Zhang P, Wang GJ, Wang B, Yao BD, Wu YP (2010) Mater Lett 64:972
40. Yang S, Song H, Yi H, Liu W, Zhang H, Chen X (2010) Electrochim Acta 55:521
41. Wen Z, Wang Q, Zhang Q, Li J (2007) Adv Funct Mater 17:2772